11nW Signal Acquisition Platform for Remote Biosensing

Alberto Gancedo, Omer Can Akgun and Wouter A. Serdijn

Section Bioelectronics, Delft University of Technology, the Netherlands

Email: a.gancedo@student.tudelft.nl, o.c.akgun@tudelft.nl, w.a.serdijn@tudelft.nl

Abstract—This paper presents the design of an extremely low-energy biosensing platform that utilizes voltage to time conversion and time-mode signal processing to sense and accommodate electrophysiological biosignals that will be later sent remotely using a simple and low power communication scheme. The electrode input is fed to a chain of monostable multivibrators used as analog-to-time converters, which create time pulses whose widths are proportional to the input signal. These pulses are transmitted to an external receiver by means of single-pulse harmonic modulation as the communication scheme, at a carrier frequency of 10 MHz. The platform is designed to be implemented in a standard $0.18\,\mu$m IC process with an energy dissipation per sample per channel of 42.72 pJ, including communication, operating from a supply voltage of 0.6V with an input referred noise of $12.3\mu V_{rms}$. The resulting SNR for OSR=256 is 35.19 dB, and the system's power consumption at a sampling and communication rate of 256 Hz is 10.94 nW.

Index Terms—EEG, low-power CMOS, time-mode operation, inductive link, ultra-low energy

I. INTRODUCTION

In remote biosensing/biomonitoring, the key challenge is the design of extremely low-energy signal acquisition platforms, which can drastically increase battery life and reduce battery size, or even enable ubiquitous energy harvesting technologies to provide enough power to operate the said platforms virtually forever.

Today, most of the circuit design is done in CMOS. The advancement and scaling of CMOS technologies has, in fact, always been based on improving digital systems' performance. Yet, with each new technology node, the supply voltage of the process node is scaled down as well, which reduces the voltage headroom that is available to the transistors for operating in saturation. Without transistors operating in the saturation region, it is very hard to realize signal processing and amplification functions in the analog domain. One possible solution to this problem is using time-mode signal processing (TMSP) techniques [1]–[4]. Time-mode operation embeds the information in the time difference between two switching events to represent an N bit signal. Compared to standard digital CMOS operation, time-mode operation is inherently more energy efficient since the number of switchings is minimized. The main drawback of these circuits, however, is the speed limitation that exists as a result of occupying time windows to represent data instead of using bits. However, low frequency operation and ultra-low power requirements make remote biosensing/biomonitoring applications a perfect fit for time-mode circuits that exploit the characteristics previously stated.

This work presents the design of an ultra-low-power remote biosensing platform, particularly tailored for EEG sensing, for which tight power-consumption and noise constraints exist. Fig. 1 shows the system-level diagram of the proposed signal chain for EEG sensing and communication. The system consists of a chain of analog-to-time converters (ATC), a communication control block that interfaces the ATC chain with the transmitter
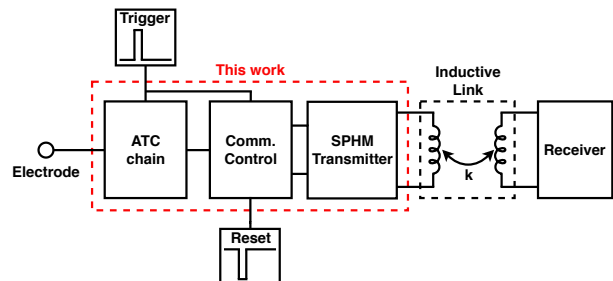

Figure 1. Proposed biosensing platform high-level block diagram

circuit, and a communication link that uses the single-pulse harmonic modulation (SPHM) scheme to transmit the sensed data.

The ATC chain converts the input voltage from the electrode to an output pulse, whose pulse-width is modulated by the electrode's signal voltage. The output of the ATC chain and the trigger signal are then fed to simple digital circuitry to create the necessary control signals for the SPHM transmitter. When the communication signal is transmitted through the inductive link, the receiver circuit generates two events per conversion (one for the rising edge and one for the falling edge of the converter's total output pulse) that represent a sampled EEG value. The time between those pulses can be converted into digital by directly interfacing the receiver to an asynchronous TDC such as in [5].

The paper is organized as follows. Section II presents the details of the proposed signal chain for EEG sensing and communication, explaining the single analog-to-time converter (ATC) operation, expanding it to a chain of ATCs, followed by the details of the communication link. Section III reports simulation results, and finally, conclusions are drawn in Section IV.

II. SYSTEM DESIGN

A. Analog-to-Time Converter (ATC)

In [6], a monostable multivibrator (MSMV) [7], as shown in Fig. 2, was used by the authors to create time-mode completion detection signals based on the sensed current consumption of digital circuits. In this work, we use a similar structure to convert the signal voltage from the electrode to a time-mode signal by modulating the current generated by pMOS transistor M1 in a similar fashion. The operation of the circuit is as follows: At the instance that a trigger pulse is applied, Node **n1** is pulled low by the NOR gate followed by Node **n2**, and the current supplied by M1 starts to charge **n2**. Once **n2** is charged to the threshold voltage of the inverter, Node **n1** goes low again, making the output high and successfully creating a pulse, that represents the sampled and converted value. The system remains in steady state (Nodes **n1** and **n2** are logic high) until the next trigger pulse arrives. As the current supplied by Transistor M1 is modulated by the input signal, the output pulse-width will be proportional to the input signal's amplitude.
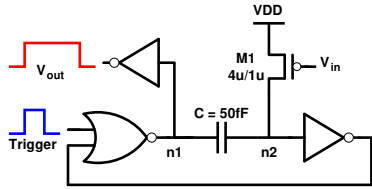
Figure 2. Monostable multivibrator circuit

Figure 4. Interface between the ATC chain and the communication circuit

Furthermore, this ATC implementation has an inherent time-out feature and will always generate a pulse event at Node **n1**, regardless of the input signal value at V_{in}, avoiding stalling of the chain. Capacitor C and Transistor M1 are made bigger than the minimum values required for correct operation to mitigate process variation effects and reduce the effect of flicker noise.

B. Oversampling ATC Chain

Due to the extremely low amplitude of the signals coming from the input electrode, oversampling and/or sharp filtering are necessary to reduce the noise levels. Oversampling is widely used in analog-to-digital converters and all sources of error and/or noise appearing with a Gaussian distribution on top of the signal will be reduced in power by a factor of 2, i.e. 3dB, per doubling of the oversampling ratio (OSR) while keeping the signal power constant [8].

An oversampling chain of ATCs is presented in Fig. 3(a). Addition of the time pulses is performed by chaining ATCs and creating a trigger signal between the ATCs using a fixed-width pulse generator (Fig. 3(b)) that activates with the falling edge of the ATC output pulse. With the addition operation of the same converted signal in the time domain (oversampling), the noise contribution is significantly reduced as a result of the noise averaging. This averaging/oversampling operation also reduces the effects of mismatch appearing in the MSMV circuit (Fig. 9) and is further discussed and backed up with simulations in Subsection III-D.

C. ATC Chain and Communication Circuit Interface

If the output of the ATC chain shown in Fig. 3(a) is monitored, only the last ATC output pulse can be seen. Therefore, a signal representing the time addition of all the ATC pulses has to be generated. For this purpose, the simple circuit shown in Fig. 4 is used. First, the trigger input to the ATC chain is captured using a positive-edge triggered flip-flop (FF). Likewise, the end of the summation operation is captured by using a negative-edge triggered FF, generating the start and finish markers of the conversion, which are then fed to an XOR gate to generate the resulting pulse, *Total ATC output*. The FFs are reset after every conversion to allow multiple samples to be transmitted.
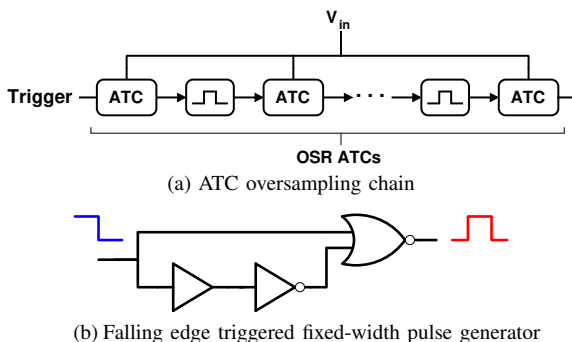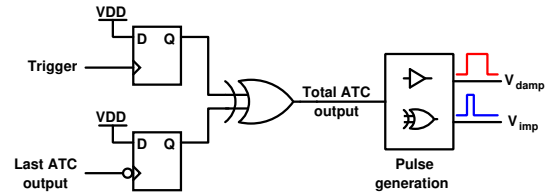
As will be presented next, pulses necessary to drive the SPHM circuitry have to be of a certain width to get the maximum performance out of the communication link. Consequently, two either-edge pulse generators, similar to Fig. 3(b) but replacing the NOR gate with an XOR gate, were used to generate the driving signals for the communication circuit out of the *Total ATC Output*.

D. Single-Pulse Harmonic Modulation (SPHM)

During the development of a remote biosensing platform with extremely low power consumption and implementation simplicity, an efficient communication system has to be considered. For these reasons, single-pulse harmonic modulation (SPHM), which can inherently make use of time-mode signals from the ATC chain, was chosen as the communication scheme and is shown in Fig. 5 (adapted from [9]).

The transmitter circuit uses one narrow pulse (fed to the gate of M_{Tx}) to create a wideband excitation that will get filtered by the high-Q LC-tank, creating a tone at the resonant frequency of the tank. Once the oscillation has built up, the pMOS switch (M_{Txd}) can be turned on to drastically lower the Q of the transmitter tank, damping the oscillation and allowing for another pulse to be sent. The receiver implementation follows a similar approach and can be as simple as an envelope detector and a thresholder circuit, reusing the output bit pulses as damping signals on transistor M_{Rxd}. According to [10], the maximum voltage swing occurs for a driving pulse width of exactly one half cycle (or an odd multiple of half cycles) of the tank's resonant frequency. Therefore, the pulse width generators described in the previous subsection were made tunable so that process variations could be compensated.

As a result of the increased pulse width with the use of oversampling in the ATC chain, the time elapsed between the two pulses transmitted per sample increases, making the width of the damping pulse on M_{Txd} less critical, thus allowing for complete damping of the tank's oscillating signal between the two transmissions per sample. The resolution achieved from the chain, when considering a noiseless scenario, will depend on the receiver's timing accuracy.

III. SIMULATION RESULTS

Characterization of the system's performance was done through transistor level HSPICE simulations, addressing the

(a) ATC oversampling chain

(b) Falling edge triggered fixed-width pulse generator

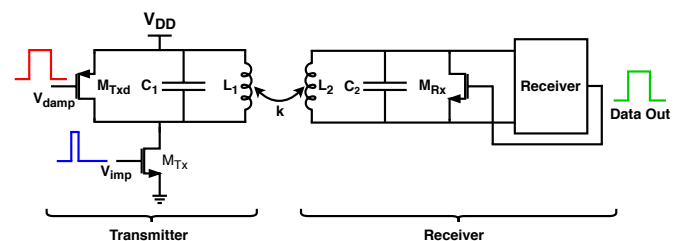Figure 3. Oversampling chain and inner trigger generation circuit

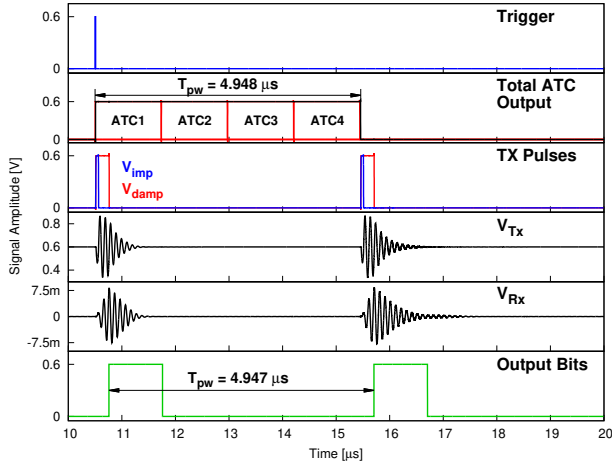Figure 5. Single-pulse harmonic modulation [9]

Figure 6. System response of the complete platform, showing the conversion starting when the trigger pulse arrives, generating a pulse at the output of each ATC (4 in this example). The total ATC output is then adapted to drive the transmitter circuit and the output bits are generated after communication using thresholding.

Figure 7. Normalized spectrum of the reconstructed output pulse, applying a signal of $1mV_{peak}$ at 100Hz to the input of the ATC chain

key points mentioned previously. Subsection III-A demonstrates the operation of the complete signal-acquisition platform, and Subsection III-B shows the performance of the ATC chain. Subsection III-C showcases the usage of the system for EEG sensing using real EEG data as the input to the ATC chain, while Subsection III-D shows the improvements on mismatch achieved by increasing the oversampling ratio. Finally, a comparison to the state of the art is presented in Subsection III-E.

A. Complete System Simulation

Fig. 6 shows the operation of the platform for a chain of four analog-to-time converters. The chain of ATCs generates the oversampled time-mode signal at the rising edge of the trigger signal and the interface circuit generates the *Total ATC Output* signal. From this signal, the driving signals for the transmitter that produce the necessary oscillation at 10MHz are generated. In this simulation, a coupling factor of k=0.005 was used to model a small coupling between the coils, and an envelope detector and a limiter with a threshold of 7.5mV was used to receive the transmitted signal and convert the received signal into a marker pulse. The pulse-width of the *Total ATC Output* pulse and the time difference between the marker pulses differ due to the differences in the driving strengths in the designed interface circuitry appearing in the reconstructed signal as a DC offset.

B. ATC Chain Performance

Dynamic performance characterization of the ATC chain was done using transistor level transient noise simulations and by means of analyzing the FFT of the reconstructed output pulse-width after applying a sinusoidal input signal of $1mV_{peak}$ over a DC voltage of 0.3V at a frequency of 100Hz. Reconstructed output signal had a SINAD of 35.19 dB, HD2 of 43.87 dB, and THD of 42.67 dB, as shown in Fig. 7. It is easily observable from the figure that, as a result of the non-differential structure used, the second order harmonic is higher than any of the higher order harmonics, as the latter are masked by the noise floor of the converter. However, higher harmonic content may arise if higher signal amplitudes are applied at the input of the current design.
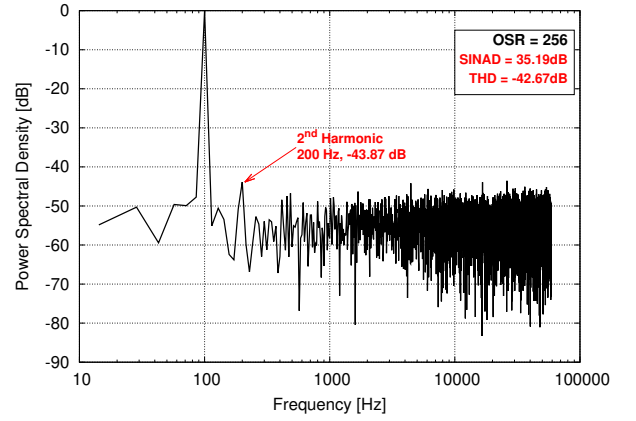
C. Correlation with Real EEG Input Data

In addition to the standard dynamic characterization, we investigated the use of the correlation factor r as a measure of the signal quality. This allowed us to pre-characterize and visually inspect the converter's performance change with respect to the increase of oversampling ratio.

Fig. 8 shows the reconstructed output signals from the ATC chain and its correlation factors to the input data sourced from [11]. It can be seen that for a low oversampling ratio of 2, none of the signal features is visually distinguishable and is practically 'buried' in noise. With higher OSR values, the converted signal begins to resemble the original input signal, and the correlation increases accordingly. Depending on the application and requirements, it may be possible to extract the necessary features from 'not so clean' biosignals and even perform analysis. This may be possible either by visual inspection or processing them with feature detection algorithms. Setting a threshold on the minimum required correlation factor for the targeted application would allow for lower power consumption.

D. Mismatch Simulations

The use of a single PMOS transistor per ATC cell as the input voltage to current converter, makes the circuit prone to mismatch. The PMOS transistor, connected to a supply of 0.6V, will operate in the near threshold (moderate-inversion) region, making the V_T variation appear as a nonlinear gain error in
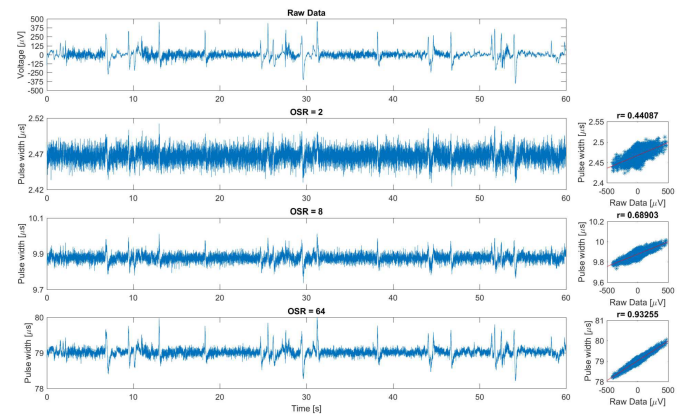

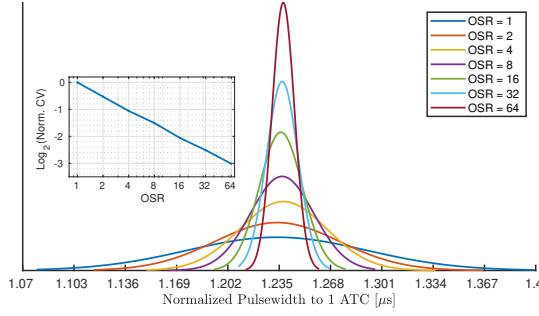Figure 8. Correlation improvement with respect to OSR

Figure 9. Mismatch improvement with respect to OSR

each ATC, where the threshold-voltage variation will be the most pronounced source of mismatch. [12] states that an inversely proportional relation with respect to area for the variance of V_T exists: $\sigma^2(V_T) \propto \frac{1}{WL}$. By chaining the ATCs sequentially instead of using a single ATC for oversampling, the effective area of the PMOS transistor will be equal to $OSR \cdot W \cdot L$, decreasing the variance (σ^2) of V_T by a factor of 2 per doubling of the oversampling ratio.

Fig. 9 shows a curve fit of the normalized probability density function over a sweep of oversampling ratios, each trace comprises of 1000 Monte-Carlo runs. The aforementioned behavior results in an improvement of 3dB per OSR doubling in its coefficient of variation ($CV = \sigma/\mu$) with respect the case of a single ATC.

E. Comparison with State of the Art

Due to its unprecedentedly low energy dissipation for a biosensing platform, the system's power consumption is orders of magnitude lower than any reported work. The summary of requirements for wearable EEG systems using active electrodes in [13] provides a set of specifications that should be met to perform reliable readouts with a wireless solution and it will be used as a reference for this paper. Similarly, [14] shows the performance requirements for neuro-recording amplifiers in implantable devices, which -in terms of power- are still orders of magnitude higher than the proposed solution.

Table I shows the energy dissipation per block of the signal acquisition platform, and its comparison to the state of the art in Table II.

IV. CONCLUSIONS

This paper presented the design and simulation results of a time-mode EEG sensing system. A chain of ATCs has been used to convert the analog voltage from the input electrode to time-mode signals, using energy-efficient and simple circuitry, where the information is later communicated to an external receiver using SPHM. The system was designed to be implemented in a standard $0.18\,\mu$m process and operating from a 0.6V

Table I
ENERGY DISSIPATION SUMMARY OF THE COMPLETE SIGNAL ACQUISITION PLATFORM

Circuit Block	Energy dissipation
ATC for OSR=256 (pJ)	5.64
Falling edge pulse generator for OSR=256 (pJ)	2.19
Communication interface (pJ)	2.31
Communication per sample transmitted (pJ)	32.58
Total energy dissipation (pJ)	42.72
Total power consumption @ fs = 256 Hz (nW)	10.94

Table II
REQUIREMENTS OF WEARABLE EEG APPLICATIONS [13], NEURO-RECORDING AMPLIFIERS [14], AND THE PERFORMANCE OF THIS WORK

Target specs per channel	[13]*	[14]**	This work
Input voltage range (mV$_{pp}$)	1	40	2
Input referred noise (μV$_{rms}$)	1	4-8	12.3
Bandwidth (Hz)	100	1-5k	1.48k
Power dissipation (nW)	100000	5000	10.94

*Wearable EEG **Neuro-recording amplifiers

voltage supply, resulting in an energy dissipation of 42.72 pJ per conversion and transmission, with $12.3\mu V_{rms}$ input referred noise over a 1.48 kHz band. While operating at a sampling and communication rate of 256 Hz, the power consumption is 10.94 nW.

REFERENCES

[1] F. Yuan, "CMOS time-to-digital converters for mixed-mode signal processing," *The Journal of Engineering*, January 2014. [Online]. Available: http://digital-library.theiet.org/content/journals/10.1049/joe.2014.0044

[2] D. Miyashita, R. Yamaki, K. Hashiyoshi, H. Kobayashi, S. Kousai, Y. Oowaki, and Y. Unekawa, "An LDPC decoder with time-domain analog and digital mixed-signal processing," *IEEE Journal of Solid-State Circuits*, vol. 49, no. 1, pp. 73–83, Jan 2014.

[3] Z. Chen and J. Gu, "Analysis and design of energy efficient time domain signal processing," in *Proceedings of the 2016 International Symposium on Low Power Electronics and Design*. ACM, 2016, pp. 100–105.

[4] O. C. Akgun, M. Mangia, F. Pareschi, R. Rovatti, G. Setti, and W. A. Serdijn, "An Energy-Efficient Multi-Sensor Compressed Sensing System Employing Time-Mode Signal Processing Techniques," in *Proceedings of IEEE International Symposium on Circuits and Systems (ISCAS)*, May 2019, pp. 1–5.

[5] O. C. Akgun, "An Asynchronous Pipelined Time-to-Digital Converter Using Time-Domain Subtraction," in *Proceedings of IEEE International Symposium on Circuits and Systems (ISCAS)*, May 2018, pp. 1–5.

[6] O. C. Akgun, F. K. Gurkaynak, and Y. Leblebici, "A Current Sensing Completion Detection Method for Asynchronous Pipelines Operating in the Sub-threshold Regime," *International Journal of Circuit Theory and Applications*, vol. 37, pp. 203–220, 2009.

[7] A. S. Sedra and K. C. Smith, *Microelectronic Circuits*, 4th ed. Oxford University Press, 1998.

[8] A. V. Oppenheim, R. W. Schafer, and J. R. Buck, *Discrete-time Signal Processing (2Nd Ed.)*. Upper Saddle River, NJ, USA: Prentice-Hall, Inc., 1999.

[9] M. Schormans, V. Valente, and A. Demosthenous, "Single-pulse harmonic modulation for short range biomedical inductive data transfer," in *2017 IEEE Biomedical Circuits and Systems Conference (BioCAS)*, Oct 2017, pp. 1–4.

[10] F. Inanlou and M. Ghovanloo, "Wideband near-field data transmission using pulse harmonic modulation," *IEEE Transactions on Circuits and Systems I: Regular Papers*, vol. 58, no. 1, pp. 186–195, Jan 2011.

[11] "CHB-MIT Scalp EEG Database," (Last accessed 10-June-2019). [Online]. Available: https://physionet.org/physiobank/database/chbmit/

[12] M. J. M. Pelgrom, A. C. J. Duinmaijer, and A. P. G. Welbers, "Matching properties of MOS transistors," *IEEE Journal of Solid-State Circuits*, vol. 24, no. 5, pp. 1433–1439, Oct 1989.

[13] J. Xu, S. Mitra, C. Van Hoof, R. F. Yazicioglu, and K. A. A. Makinwa, "Active electrodes for wearable eeg acquisition: Review and electronics design methodology," *IEEE Reviews in Biomedical Engineering*, vol. 10, pp. 187–198, 2017.

[14] H. Chandrakumar and D. Markovic, "An 80-mvpp linear-input range, 1.6GΩ input impedance, low-power chopper amplifier for closed-loop neural recording that is tolerant to 650-mvpp common-mode interference," *IEEE Journal of Solid-State Circuits*, vol. 52, no. 11, pp. 2811–2828, Nov 2017.